Results from the G^0 engineering runs. (Answers to the certification questions.)

The G^0 collaboration.

March 5, 2004

Abstract

Information describing the present G^0 collaboration understanding of the data taken during the two G^0 engineering runs are presented. From the data taken so far, the expectations for the results of production run are presented. As a results of those two runs, the G^0 collaboration is confident that the experiment will meet its scientific goals as presented to and approved by the PAC.

Contents

1 Beam properties. 5

2 Beam feedbacks, helicity ground loops. 7

3 Apparatus sensitivities to beam for the G0 experiment. 13

4 False asymmetries as a product of beam properties and apparatus sensitivities. 20

5 Questions related to physics background. 23

6 Status of the electronics, dead-time, noise to counting statistic. 31

7 Status of Y_0 timing. 39

8 Current Dependence of Beam Polarization. 42

9 Experience reliability. 46

10 Conclusion. 46

In order to certify that the G^0 experiment will achieve its scientific goals, the G^0 collaboration has been asked to answer questions put together by the management of the Physics Division at JLab. In this document, all issues raised by those questions are answered though they might not be in the same order than the original question list. The original question are repeated in the following lines. The sections that address the issues are referenced.

List of "certification" questions from JLab :
Will the G0 experiment meet its scientific goals as presented to and approved by the PAC?

1. *Do the helicity correlated beam parameters meet specification? If not, how far off are they, and is this acceptable? (see section 1)*
2. *Do the measured sensitivities of the G0 apparatus to the beam properties match specifications and/or expectations? If not, how far off are they, and is this acceptable? (see section 3)*
3. *Are the false asymmetries clearly explained as a product of the beam properties and apparatus sensitivities? (see section 4)*
4. *How stable are the beam properties and apparatus sensitivities with time? (see section 3)*
5. *Given the measured performance of both the accelerator and the G0 equipment, how do the anticipated data uncertainties, as function of Q^2, compare to the proposed uncertainties? In particular:*
   (a) *Given the measured helicity-correlated beam parameters and apparatus sensitivity (and their stability over time), how big will the systematic errors be in the final experiment result? (see section 3)*
   (b) *Given data rates, backgrounds, and other experiment issues (and their stability over time), how big will the statistical errors be in the final experimental result? (see section 5)*
6. *Are all required feedback loops in operation and stable? Is the experiment sufficiently electrically isolated from the helicity generating sources? (see section 2)*

7. *What is the background situation under the elastic peak, both in magnitude and in helicity dependence. What are the plans to mitigate/measure/subtract this background? What impact will backgrounds have on the final anticipated uncertainty of the measurements, as a function of Q^2. (see section 5)*

8. *What is the status of the custom detector electronics, both the North American and the French? Can helicity correlated dead time seen by the French electronics be reconciled with dead time observed in the North American electronics. What is the noise to counting statistics ratio of these systems? (see section 6)*

9. *What is the status of the "YO" timing? Is it clear that using this as a common stop to the TDC's benefits the experiment? (see section 7)*

10. *During the second engineering run a test is planned to measure the beam polarization ranging from low current measurements to high current production runs. If this test was successful, is there any quantitative change to the beam polarization at high current, and if so, will it affect the G0 data quality? (see section 8)*

11. *Has the G0 equipment performed sufficiently reliable for a full production run to take place? (see section 9)*

1 Beam properties.

Question 1 : Do the helicity correlated beam parameters meet specification? If not, how far off are they, and is this acceptable?

The helicity correlated beam parameter specifications have been met through a collaborative effort of the accelerator division and the G^0 collaboration. Briefly, achieving the parity quality specifications required a combination of rotating half-wave plate optimization, helicity Pockels cell voltage tuning, charge feedback with the IA cell, position feedback with the piezoelectric mirror(PZT), minimization of the charge asymmetry on the Hall A beam with their IA cell, and some fine tuning of quadrupoles in Hall C to optimize the response of the PZT feedback system at our target. Despite the fact that the parity quality specifications are being met, the feedback systems continue to require some degree of attention that uses some of our beam time almost on a daily basis. Further information about the operation of the feedback systems is contained in section 2.

Data on the helicity-correlated beam properties for two distinct periods are shown in Table 1. In December 2003, the only beams routinely in the machine were the nominal Hall B beam and 40 μA of G^0 beam. With the feedback loops operational, all helicity-correlated beam specifications were satisfied during this period. In early January 2004, the Hall A 100 μA beam with its stringent energy spread requirements was added. Without going into all the details, much time was spent to achieve compatible running conditions for the two beams. The major observation was the influence of charge asymmetry in the Hall A beam on the G^0 beam's helicity-correlated position and energy differences. This was taken care of by setting up a feedback loop using the Hall A IA to insure that the charge asymmetry on the Hall A beam was small. Compatible running between G^0 and Hall A 100 μA beam was achieved on Jan. 20. Data from that period until Jan. 26 is shown in Table 1. During this period G^0 was running primarily with 20 μA of beam to satisfy the collaboration's primary goal of collecting empty target data. The helicity-correlated beam parameter specifications were met during this period, as well.

We have not yet demonstrated that the parity specifications can be achieved with 40 μA of G^0 beam and 100 μA of Hall A beam simultaneously, but it is likely that it can be done since we have not seen significant differences in our IA and PZT calibration parameters between 20 and 40 μA.

Table 1: *Average of helicity-correlated beam parameters over all runs for two run periods. The December 2003 period represents about 77 hours of data with 40 μA of G^0 beam and no Hall A beam. The January 2004 period represents about 46 hours of data with 20 μA of G^0 beam and 100 μA of Hall A beam. The parameters are the charge, position and angle projected to the target, and the relative energy. The last row shows the desired specifications – all quantities in this table presently meet these specifications.*

Date	$\Delta Q/Q$ (ppm)	Δx (nm)	Δy (nm)	$\Delta\theta_x$ (nrad)	$\Delta\theta_y$ (nrad)	$\Delta E/E$ ($\times 10^8$)
Dec. 2003	-0.5 ± 1.4	5.7 ± 7.7	7.1 ± 8.5	1.3 ± 0.7	0.5 ± 1.1	0.6 ± 0.6
Jan.2004	-0.6 ± 0.3	-3 ± 15	-1 ± 21			
spec.	1	20	20	2	2	≤ 2.5

2 Beam feedbacks, helicity ground loops.

Question 6: Are all required feedback loops in operation and stable? Is the experiment sufficiently electrically isolated from the helicity generating sources?

The feedback loops used by G^0 are all aimed at minimizing helicity-correlated beam properties. They include the Hall C IA to control the charge asymmetry, the Hall C piezo-electric (PZT) mirror to control the position differences, and the Hall A IA to control the charge asymmetry on their beam, which has been observed to influence the Hall C helicity-correlated position and energy differences. The feedback algorithm used takes account of the fact that the IA system has some effect on position differences and the PZT system has some effect on charge asymmetries. It takes much less time to accurately measure charge asymmetries, so adjustments to the IA are made after integration times of 5 minute, while adjustments to the PZT are made after integration times of 30 minutes.

Figure 1 shows results of the operation of the feedback system over the course of 5 hours with all three feedback systems in operation. In this particular case, one can see that the feedback system brought an initial charge asymmetry of $\sim$ 14 ppm and x position difference of $\sim$ 750 nm to within specifications. Since Jan. 20, the feedback loop has been operational and the helicity-correlated beam specifications have been achieved. However, maintaining this level of performance requires some degree of attention that impacts our beam time almost on a daily basis. For example, on Jan. 23 the response of the PZT system as measured at our target got very small, for undetermined reasons. The response was so small that it was no longer possible to use the system to correct the position differences. Various things were tried to recover the response; finally after about 3 hours it was found that tuning quadrupoles in the hall C line was able to bring the PZT responses back up to levels that would allow the feedback system to operate. This involves a trade-off, because increasing the PZT response typically increases our position difference '"noise" (width of our helicity-correlated position difference distributions) and sometimes the beam halo. Increasing the position difference noise causes the feedback to take a longer time to converge. On Jan. 24 and Jan. 25, it was found that the changes of Jan. 23 made the halo too large. So more tuning was done to simultaneously get acceptable PZT slopes, beam position difference noise, and halo. Tuning the quadrupoles to

fix this problem is probably just compensating for something else that has changed in the accelerator, so we are continuing to work with the accelerator division to determine the root cause of the PZT response changes. In summary, successful operation of the feedback systems involves a delicate balance of many different factors. A continued effort to understand the root causes of the drifts is warranted, because in the long run it will likely reduce the need to use beam time to try to maintain the delicate balance.

The second part of this question asks whether or not the experiment is sufficiently electrically isolated from the helicity-generating sources. The experiment uses the delayed helicity reporting technique to report the state of the helicity signal to the halls; this insures that the "in-time" helicity signal is not present in the electronics in the experimental halls. It does not insure that the experimental electronics is necessarily completely isolated from the helicity-generating sources like the helicity Pockels cell and the pseudo-random helicity generation circuit that drives it. Direct measurement is needed to verify isolation at the needed level. To answer this question, we must consider the two types of electronics in the G^0 experiment - integrating and pulse counting - separately.

First we consider the integrating electronics. This is how the signals from the beam charge monitors (BCM), beam position monitors (BPM), luminosity monitors, and halo monitors are treated. These are all voltage signals, and they are sent to voltage-to-frequency converters (V/Fs). The outputs of the V/Fs are sent to scalers and recorded every 33 msec. The procedure for directly measuring the isolation here is straightforward - one takes data with no beam but the helicity generating sources in operation. The random electrical noise (at the reversal frequency) in these circuits is small enough that a significant limit can be set in a short amount of data-taking. The top two panels of Figure 2 show the measured helicity-correlated asymmetry for the BCM1 and BCM2 electronic chains. To define an asymmetry here, a "noiseless" signal in software with an amplitude corresponding to 40 μA beam is added in to the recorded electronic fluctuations during the run. Then the asymmetry is computed and plotted in the normal way. For the two BCM channels values of $-.04 \pm .06$ ppm and $-.06 \pm .05$ ppm are found after about 3.5 hours of running. This limit is smaller than our smallest expected statistical error for the main detector of ~ 0.3 ppm. We will monitor the possibility of helicity-correlated electronic signal pick-up in our integrating electronics continuously during our 700 hour production run with two channels instrumented with batteries and one channel terminated in the hall in a

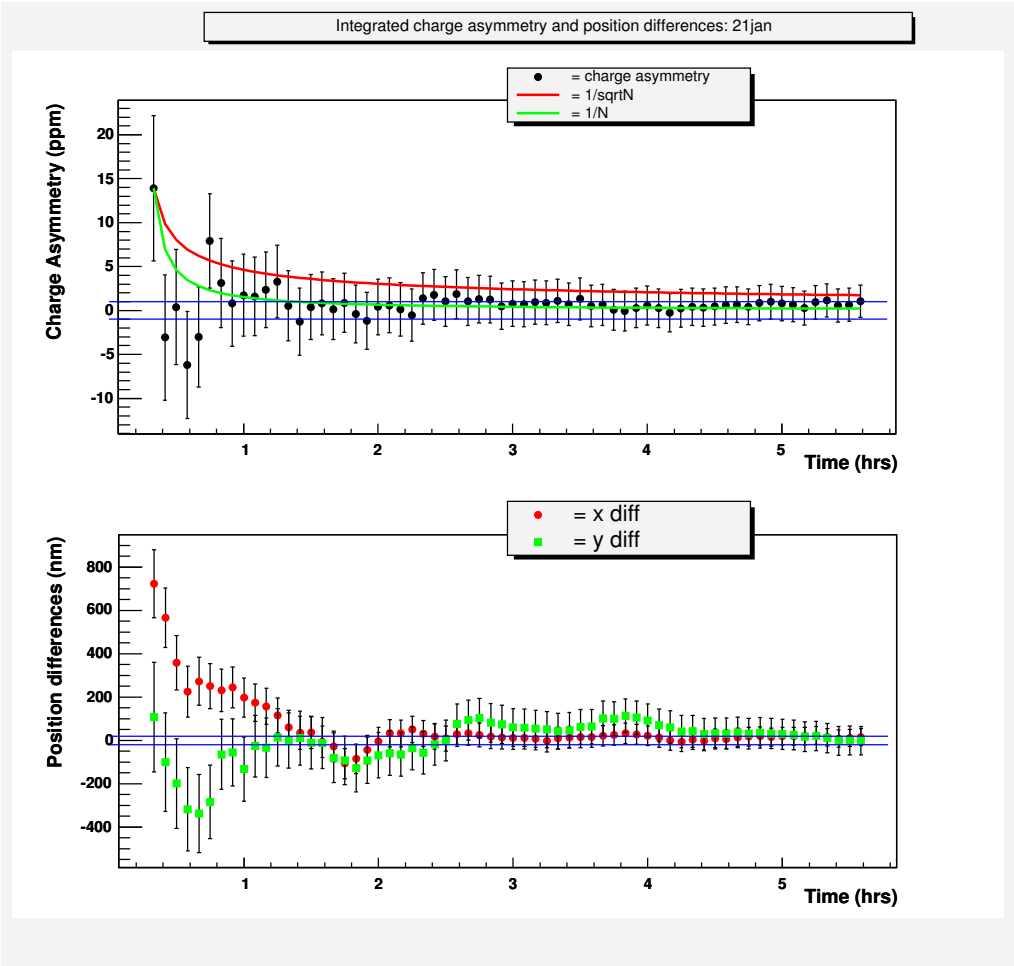

Figure 1: *Results for the integrated charge asymmetry and x and y position differences at the target over the course of about 5 hours with all three feedback systems running. The integrated values are plotted every 5 minutes. Actual changes to the intensity (Hall C IA) feedback loop are done every 5 minutes, while changes to the position (Hall C PZT) feedback loop are done every 30 minutes. The solid horizontal blue lines indicate the desired specification range on the helicity-correlated parameters. The line labeled $1/N$ shows that the charge asymmetry feedback is following the expected $1/N$ fall-off, where N is the number of updates since the feedback loop was started. The line labeled $1/\sqrt{N}$ (statistical reduction) is included for reference.*

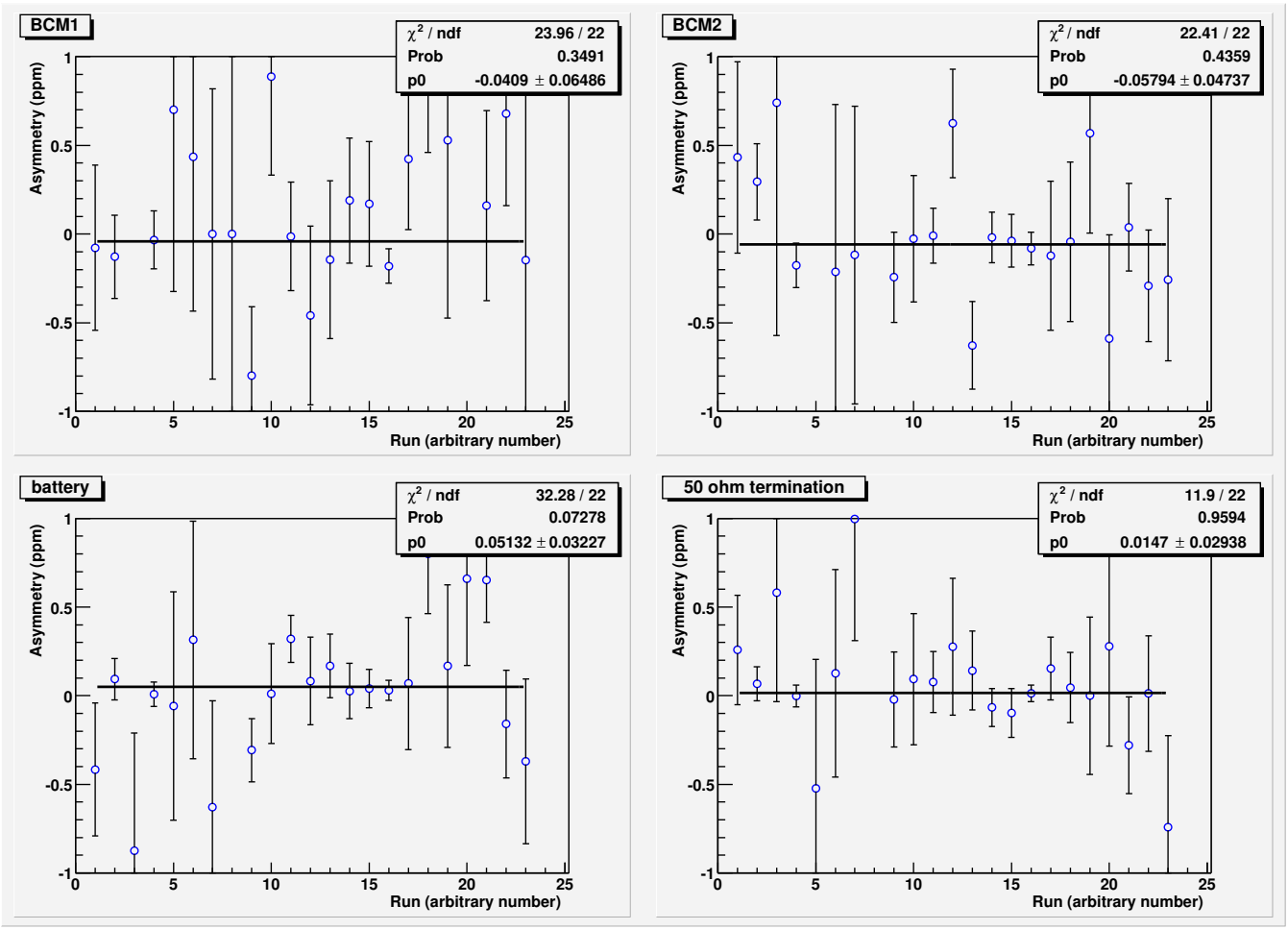

Figure 2: *Helicity-correlated "asymmetries" for four different integrating-mode electronic channels with beam off. The definition of the asymmetry is contained in the text. The channels correspond to two beam charge monitor channels, a channel with a battery attached, and a channel with a 50 ohm terminator attached. The displayed data represents about 3.5 hours of data of this type. The results are statistically consistent with zero, indicating no pickup of the helicity-generating electronic signals at this level.*

50 ohm terminator.

For the pulse-counting electronics, we must make an indirect argument to show that we are sufficiently isolated from the helicity generating electronics. Pulse-counting electronics refers to the electronic chain followed by our photo-tube signals from the focal plane detectors (FPD). These signals go into discriminators; the concern is whether or not the voltage signals going into these discriminators are sufficiently isolated from the helicity-generating sources. To address this question, we set up two electronic chains that follow the electrical path of the FPD photo-tubes very closely. One is a battery mounted on the G^0 ferris wheel hooked to the same type of signal cable as the FPD photo-tubes. The other is the same type of cable but terminated in a 50 ohm terminator at the ferris wheel patch panel. These two signals follow the same path as the FPD photo-tube signals, except when they reach the G^0 cage where these two signals go into V/F's to look for possible helicity-correlated pick-up in the voltage. The results are shown in the two lower panels of Figure 2 for the battery and 50 ohm terminator. The 50 ohm terminator results can be translated into a value of 0.1 ± 0.4 μV for the helicity-correlated voltage difference. Assuming the same limit at the input to the discriminators implies $< 0.5\mu$V helicity-correlated voltage difference in the signals. Such a variation would only have an impact on the counting rate near discriminator threshold. Most of the pulses from our primary protons of interest are well above threshold. This is illustrated in Figure 3, which shows a typical pulse height spectrum in one of the FPD scintillators cut on the elastic proton timing peak. We can make a quantitative estimate - the fractional change in the number of recorded counts for variations of the voltage near threshold is $\frac{1}{N}\frac{dN}{dV} \sim 0.002$ V^{-1} for a typical FPD detector. This leads to an upper limit on the possible false asymmetry of 0.001 ppm, which is small compared to our expected smallest statistical errors of about 0.3 ppm.

It is not adequate to demonstrate absence of pickup of the helicity-generating signal at one instant in time. We intend to measure it continuously throughout the production run. We will do two things in addition to the standard insertable half-wave plate reversals which measure these effects. For the integrating electronics, it will be done with the battery and 50 ohm channels in the V/Fs as already described. For the pulse counting electronics, we will have a second Pockels cell on the laser table driven by a pseudo-random helicity sequence that is offset by one from the usual sequence. The "electrical environment" of the second Pockels cell will be

made as identical to the electrical environment of the primary Pockels cell as possible. The only difference will be that the second Pockels cell will not be in the laser beam, so it could only influence our experiment through an electronic coupling. We will search in our FPD data for a correlation with the second Pockels cell; absence of such a correlation will allow us to set an upper limit on this type of coupling.

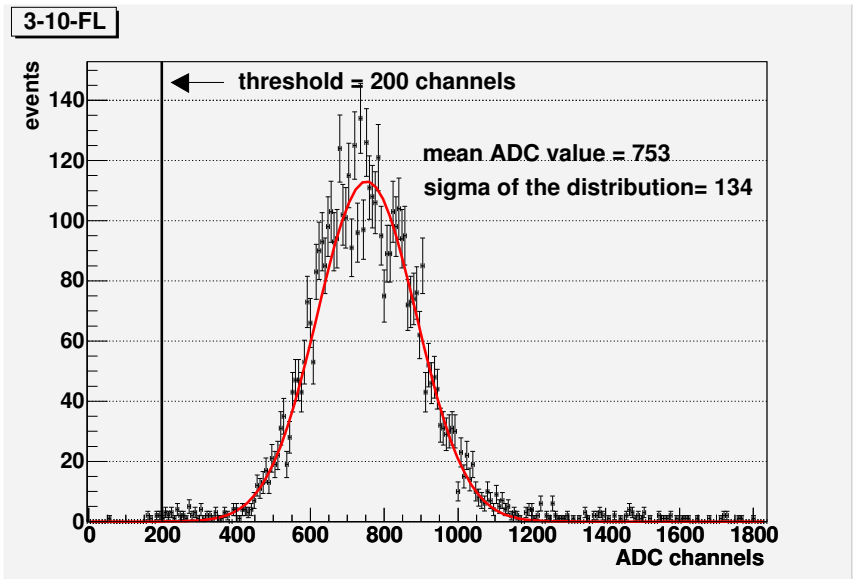

Figure 3: *Typical pulse height spectrum for events firing an FPD scintillator that are within the elastic proton timing cuts.*

3 Apparatus sensitivities to beam for the G0 experiment.

Question 2 : Do the measured sensitivities of the G0 apparatus to the beam properties match specifications and/or expectations? If not, how far off are they, and is this acceptable?
Question 4 : How stable are the beam properties and apparatus sensitivities with time?
Question 5a : Given the measured helicity-correlated beam parameters and apparatus sensitivity (and their stability over time), how big will the systematic errors be in the final experiment result?

We observe the sensitivities of the G0 apparatus to six beam properties. These properties include the helicity correlated x and y beam motion, x and y beam angle, beam energy, and beam charge. The helicity correlated beam position and angle differences are calculated using two BPMs closest to the G0 target. The energy difference is measured using a BPM in the dispersive region in the arc. Finally, the beam charge is measured from the standard HallC BCMs.

To characterize the sensitivities of the G0 apparatus to the beam properties, we observe the variation in yield in our detectors to changes in these beam properties. The sensitivities of each octant to changes in beam parameter can be seen on figure 4. What is seen is the percent change in yield on our detectors as the beam properties are varied. In general, diametrically opposing octants should have opposing sensitivities (signs) to changes in beam position and angle. The above plot shows just such a sine shaped behavior when one observes the slopes over the octants. The asymmetries for G0 are calculated by taking the mean asymmetry over all octants, so the same must be done to measure the false asymmetry contributions coming from the apparatus sensitivities. Due to this sine shaped behavior, the sensitivities due to changes in beam position and angle are canceled out between diametrically opposing octants when one takes the mean. The resulting octant-averaged slopes as well the false asymmetries they generate are shown on table 2 for the insertable half-wave plate (IHWP) OUT and table 3 for the IWHP IN. This gives rise to a cumulative false asymmetry correction of -0.004 ppm for the IHWP OUT state and -0.102ppm for the IHWP IN state. The charge asymmetry and position differences are expected to decrease as the G0 charge

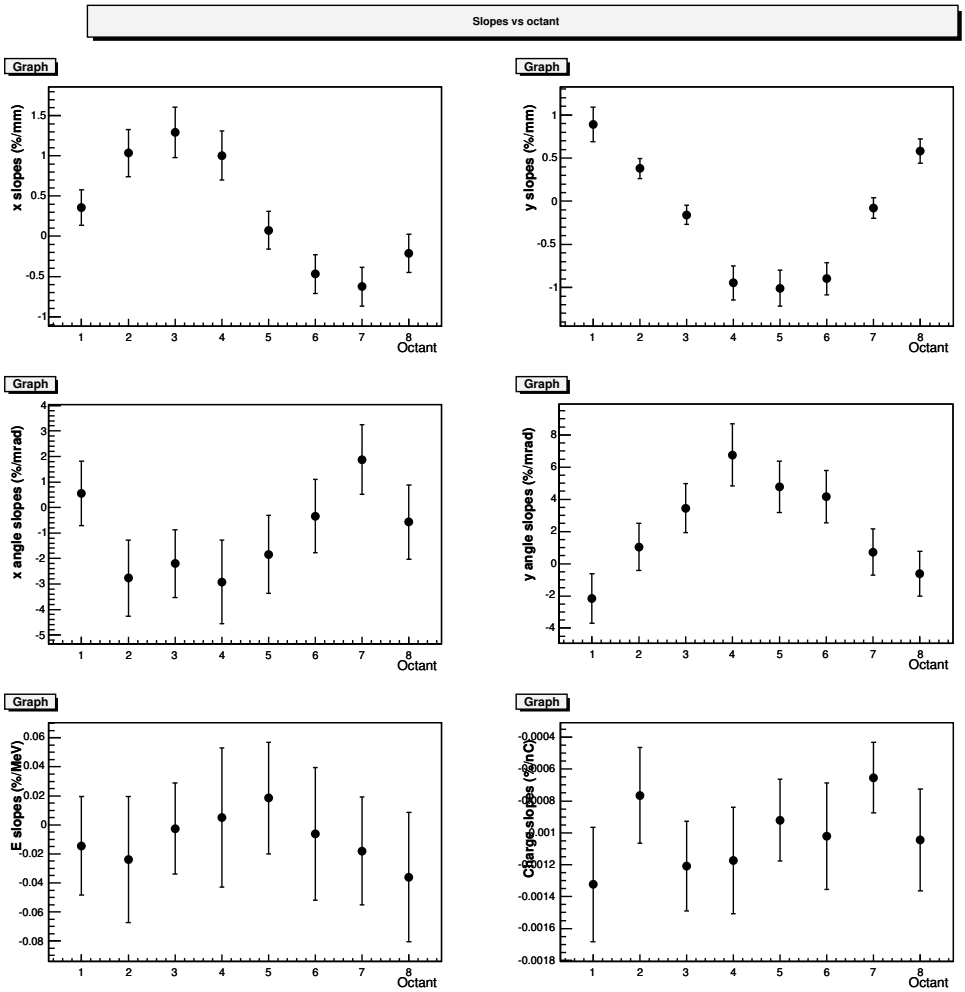

Figure 4: *Detector sensitivity slopes plotted as a function of octant.*

Beam Parameter	x position	y position	x angle	y angle	Energy	Charge
Octant-averaged Slopes	0.23 %/mm	-0.14 %/mm	-0.79 %/mrad	1.83 %/mrad	0.03 %/MeV	-0.0009 %/nC
Helicity correlated differences	7.8 nm	3.8 nm	1.4 nrad	0.8 nrad	22.6 eV	0.53 ppm
False Asymmetry Correction	0.018 ppm	-0.005 ppm	-0.011 ppm	0.015 ppm	-0.007 ppm	-0.006 ppm

Table 2: *IHWP OUT false asymmetries. The data are from 38 asymmetry runs taken during the December portion of the 2003-2004 G0 engineering run. It should be noted that not all of the above runs were taken with the feedback on, or with the charge asymmetries and position differences converged to within specifications.*

Beam Parameter	x position	y position	x angle	y angle	Energy	Charge
Octant-averaged Slopes	0.43 %/mm	-0.37 %/mm	-3.05 %/mrad	2.95 %/mrad	-0.06 %/MeV	-0.00098 %/nC
Helicity correlated differences	3.8 nm	10.0 nm	1.3 nrad	-0.35 nrad	6.8 eV	-2.1 ppm
False Asymmetry Correction	0.016 ppm	-0.037 ppm	-0.040 ppm	-0.01 ppm	-0.004 ppm	-0.027 ppm

Table 3: *IHWP IN false asymmetries. The following data are from 21 asymmetry runs taken during the December portion of the 2003-2004 G0 engineering run.*

and position feedback runs for a longer duration.

We have not yet measured the helicity-correlated beam size variations. We are developing a method to do this using the harps on the G0 girder in collaboration with members of the Accelerator Division who are working on similar measurements in the injector. Based on a simple estimate of the change in solid angle, we expect the sensitivity of the yield to beam size changes is of order $3 \times 10^{-10}/\mu m$; therefore, even helicity-correlated changes on the order of the intrinsic beam size of ~ 100 μm will give a small effect.

The stability of the slopes has been monitored throughout the engineering run. It has been observed that there seem to be some "non-statistical"

fluctuations accompanying the slopes of each octant (the slopes for all octants move together as a function of time). Figure 5 shows the slopes of all 8 octants over time.

The problem concerns the fact that the slopes from all 8 octants fluctuate "together" on occasion, beyond what can be explained by the calculated statistical uncertainties. This "non-statistical" fluctuation is not well understood at the moment, although as explained in the following section, this variation is small enough to be unimportant.

The error associated with the slopes (and naturally, the false asymmetries) should take into account these fluctuations. This is done conservatively by taking the standard deviation of the fluctuation of the slopes over time, and characterizing that as being the uncertainty on the slopes. The error on the false asymmetries taking into account the fluctuations of the slopes as well as the error on the helicity correlated beam parameters can be seen on tables 4 (IHWP OUT) and 5 (IHWP IN). The cumulative error on the false asymmetries taking into account the fluctuation of the slopes as well as the error on the helicity correlated beam properties is 0.044ppm (IHWP OUT) and 0.113ppm (IHWP IN).
At present, both the helicity correlated beam parameters as well as the slopes are statistically limited, with the errors being comparable to the mean values. With improved statistics, the errors on the false asymmetries are expected to decrease. Furthermore, even without the improved statistics, the above uncertainties on the false asymmetries are already a factor of 1.5 to 3 less than the smallest statistical uncertainty of 5% of the physics asymmetry achieved after 700 hours of running.

Another potential contribution to the systematic uncertainty of this correction procedure, can be due to the fact that, there exists some unmeasured beam parameter, which is correlated with the detector, and has helicity dependence. This would manifest itself as a non-zero lumi asymmetry, after all corrections have been applied. For the FPDs, in principle, one should then find the correlation between the asymmetries of FPDs and lumis and fold with the residual lumi asymmetries as

$$\Delta A_{sys} = \frac{\partial A_{FPD}}{\partial A_{Lumi}} A_{Lumi}. \tag{1}$$

Within our present limited statistics, we do not observe a correlation between the lumi and FPD asymmetries. For completeness, we just scale the

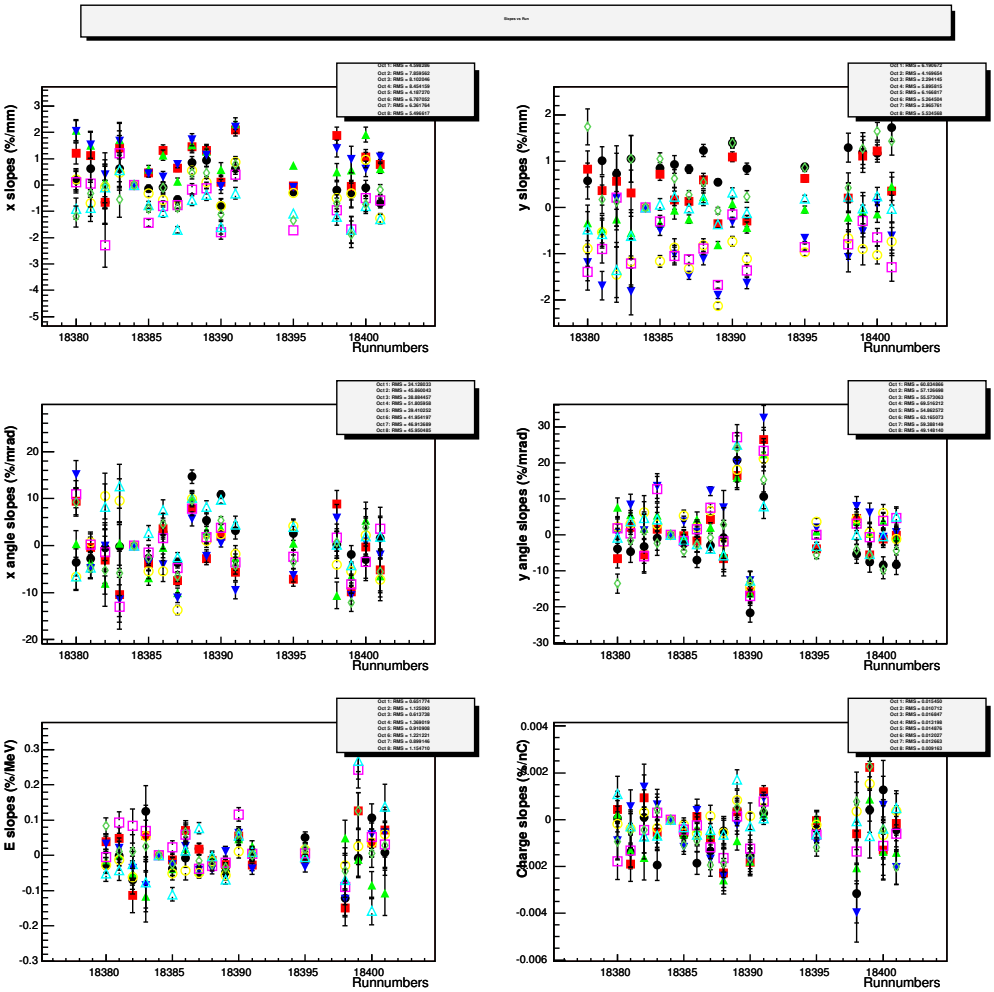

Figure 5: *Detector sensitivity slopes plotted as a function of run number. The sinusoidal shapes for the position and angle responses simply reflect the increase or decrease of the solid angle; the sign difference in, e.g. x and θ_x is due to an arbitrary choice of positive directions. These slopes are from the December run; their stability as a function of run number has improved since then.*

Beam Parameter	x position	y position	x angle	y angle	Energy	Charge
Stdev/sqrt(N)	0.09 %/mm	0.06 %/mm	0.55 %/mrad	0.66 %/mrad	0.02 %/MeV	0.0002 %/nC
Uncertainty in Helicity correlated differences	9.5 nm	9.2 nm	0.93 nrad	1.4 nrad	23.2 eV	1.68 ppm
Uncertainty in False Asymmetry Correction	0.023 ppm	0.013 ppm	0.011 ppm	0.026 ppm	0.008 ppm	0.02 ppm

Table 4: *IHWP OUT false asymmetry uncertainties coming from the fluctuation of the slopes. These uncertainties will be reduced as the uncertainties in the helicity-correlated differences are reduced.*

Beam Parameter	x position	y position	x angle	y angle	Energy	Charge
Stdev/sqrt(N)	0.25 %/mm	0.14 %/mm	1.2 %/mrad	1.0 %/mrad	0.03 %/MeV	0.0002 %/nC
Uncertainty in Helicity correlated differences	14 nm	18.8 nm	0.92 nrad	1.6 nrad	18.2 eV	2.2 ppm
Uncertainty in False Asymmetry Correction	0.06 ppm	0.07 ppm	0.032 ppm	0.047 ppm	0.011 ppm	0.03 ppm

Table 5: *IHWP IN false asymmetry uncertainties coming from the fluctuation of the slopes. These uncertainties will be reduced as the uncertainties in the helicity-correlated differences are reduced.*

residual lumi asymmetry we have measured so far by the expected statistical precision in 700 hours, as conservative estimate of a systematic error associated with the corrections procedure (see Fig. 7).

$$\Delta A_{sys} \sim A_{Lumi} \times \frac{\sqrt{31.5 \text{ hrs}}}{\sqrt{700 \text{ hrs}}} = 0.46 \text{ ppm} \times 0.21 = 0.1 \text{ ppm} \qquad (2)$$

This is significantly smaller than the expected statistical uncertainty of the FPD asymmetries (~ 0.3 ppm per FPD ring).

4 False asymmetries as a product of beam properties and apparatus sensitivities.

Question 3 : Are the false asymmetries clearly explained as a product of the beam properties and apparatus sensitivities?

The detector sensitivity to the beam properties and the related false asymmetry correction have been discussed in the answer to question 2 (see section 3). Here we argue from a slightly different perspective, using the luminosity detectors. Because these detectors are very forward angle($\sim< 2°$), they are likely more sensitive to the beam properties than are the focal plane detectors. In addition, the average Q^2 of events in the lumi detectors is very low, so the parity violating asymmetry (Moller, e-p and e-Al elastic) measured by these detectors is estimated to be $<\sim 0.1$ ppm. Therefore any nonzero asymmetry seen by these detectors can be associated with beam-induced false asymmetries.

As with the FPD analysis described in section 3, we use a multi-dimensional linear regression method to compute the luminosity detectors' sensitivities (slopes) to the beam properties. The correlation slopes, multiplied by the helicity correlated beam properties, were applied to correct for the false asymmetries as

$$A_{corr} = A_{raw} - \sum_k \frac{\partial Y}{\partial P_k} \frac{P_k^+ - P_k^-}{2Y} \,, \tag{3}$$

where P_k are a set of beam properties, Y is the detector yield, and $\frac{\partial Y}{\partial P_k}$ are the correlation slopes.

Fig. 6 demonstrates the effectiveness of this correction procedure. The measured asymmetry of a lumi detector is plotted against the helicity correlated beam properties, during a set of calibration runs, in which the Hall C IA voltage was varied deliberately to create large charge asymmetry ($\sim \pm 2000$ ppm) and position differences ($\sim \pm 2\ \mu m$). One sees that rather large false asymmetries are removed after the correction. We note that for this analysis the linear regression procedure was improved by reducing the number of beam parameters to the three (x,y and charge), rather than the usual six (x,θ,y,ϕ,E,charge); with the very large induced beam charge asymmetry, inclusion of the other parameters appears only to add noise to the regression.

Fig. 7 shows the average asymmetries, of the 7 individual detectors, from 53 runs ($\sim$ 31.5 hrs) taken in Dec. 2003. The asymmetries have been cor-

rected for sign of the electron spin (IHWP IN/OUT), as well as the six beam properties used in the FPD linear regression. The $\pm 1\sigma$ error band of the fit shown on the plot, takes into account the correlations of the individual error bars, due to common statistical uncertainties such as target density fluctuations. The net asymmetry is 0.46 ± 0.33 ppm, which is consistent with zero to 1.5σ.

We therefore believe that the false asymmetry can be attributed to the product of the apparatus sensitivity to the measured beam properties.

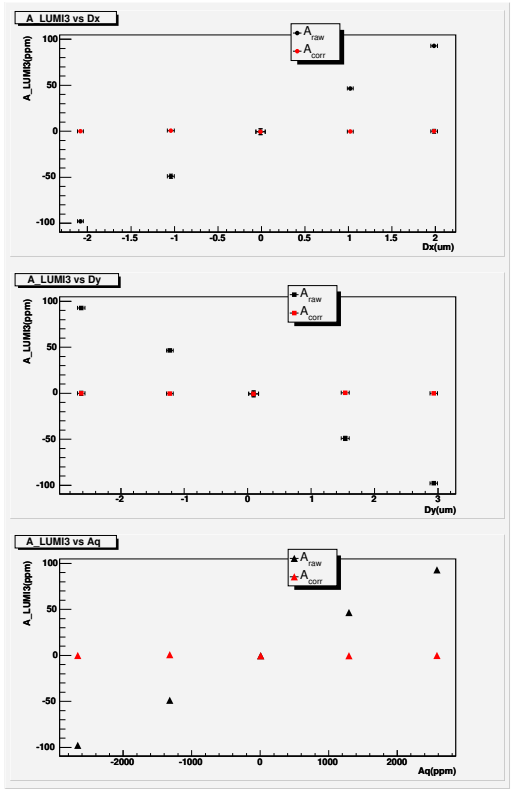

Figure 6: *Raw and corrected Lumi asymmetry vs. Dx, Dy, and Aq during the IA scan.* $Aq \sim \pm 2000$ *ppm,* Dx*,* $Dy \sim \pm 2$ μm

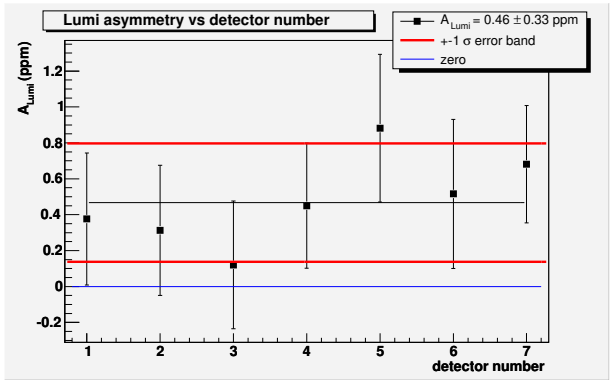

Figure 7: *Average asymmetry measured by individual lumi detectors. Black: data points and fit. Red:* $\pm 1\sigma$ *error band (the correlation between the statistical uncertainties in between different lumis has been taken into account). Blue: Zero.*

5 Questions related to physics background.

Question 5b : Given data rates, backgrounds, and other experiment issues (and their stability over time), how big will the statistical errors be in the final experimental result?

Question 7 : What is the background situation under the elastic peak, both in magnitude and in helicity dependence. What are the plans to mitigate/measure/subtract this background? What impact will backgrounds have on the final anticipated uncertainty of the measurements, as a function of Q^2.

During the January 2003 engineering run, it was realized that a 13-25% background was present beneath the elastic peak in the time-of-flight (TOF) spectra. The background fraction rose with higher detector number and therefore Q^2. Additionally, it was realized that the asymmetry in the sidebands was significant, of order 10 ppm. In spring 2003, it was estimated that a significant fraction of this background would arise due to an effect that had not been considered previously for G^0: photo-disintegration of quasi-deuterons in the aluminum target windows. Substantial effort was undertaken by the target group to both reduce this background (by thinning the target exit window) and to provide tools to study this background (by designing and constructing radiator and dummy targets). The exit window was successfully thinned from 11 mils to 3 mils. (The entrance material – two aluminum windows of 7 and 9 mil thickness plus 16 cm of He gas – gives a background contribution which is now roughly comparable to that of the thinned exit window.) An insertable 2.4% tungsten radiator was mounted to the target apparatus upstream and out of the acceptance of the spectrometer. A 30 mil aluminum foil dummy target (the "flyswatter"), was mounted to an arm so that it could be inserted a few centimeters downstream of the target exit window. The intended purpose of the radiator and flyswatter were: a) to confirm the expected fraction of events from the downstream window, and b) to be able to quickly collect asymmetry data on aluminum to the level of a few ppm in a short amount of time.

At the beginning of the December 2004 run period, it was immediately recognized that the background due to the target exit window had been reduced. The overall background underneath the elastic peak was found to be 8-15% in accord with expectations. Short studies using the radiator

and flyswatter targets were also performed. A comparison of the data to first principles Monte Carlo predictions was performed, and the Monte Carlo rates were found to underestimate the data at the 30% level (similar to the level of agreement ultimately achieved for the January 2003 data). The current level of agreement between the Monte Carlo and data is displayed in Fig. 8. Through comparisons of various target configurations (e.g. LH_2 with flyswatter vs. radiator with flyswatter, and LH_2 target vs. gaseous target) we believe the fraction of events arising from each part of the target in the beam (upstream window, downstream window, and LH_2 itself) will be understood with sufficient confidence. For example, the fraction of events due to the target windows can be estimated by appropriate rescaling of empty target and flyswatter data. The result is displayed in Fig. 9.

The flyswatter target became inoperable, stuck in the out-of-beam position, before a significant amount of asymmetry data could be acquired. For this reason, the remainder of the engineering run has been focused on the commissioning of other tools for the acquisition of asymmetry data in a reasonable amount of time on aluminum targets. The targets available to us are: the target cell itself, which must be filled with gaseous cold hydrogen (GH_2) for cooling, and a 3 mm thick aluminum frame mounted on top of the target and upstream of the target entrance window, which is normally used for diagnosis of beam halo. The GH_2 target has been commissioned at 20 μA, and the Al frame target at 15 μA, limited by beam heating. It has been estimated that two weeks of running on the GH_2 target and two days of running on the Al frame target would be sufficient to achieve a 3 ppm statistical uncertainty on asymmetries from these sources. The times may be reduced if these targets can be run at higher current.

Initial analysis of asymmetries from running so far have shown that the GH_2 data and Al frame data are consistent with one another. The magnitude of the asymmetries range from roughly -20 ppm in the lower detectors to zero ppm in the higher detectors (within the as yet large statistical uncertainties). This is in good agreement with expectations based on analysis of asymmetries in the sidebands of the proton peak from regular LH_2 running.

Given the fractions of events arising from physics backgrounds and their systematic uncertainties, we estimate an effective increase of the LH_2 statistical uncertainty by no more than 50%. The dominant contribution to the total uncertainty would still be the statistical uncertainty on the LH_2 measurement, with the statistical uncertainty of the GH_2 and Al asymmetry measurements being second. Comparison of the GH_2 and Al frame asymme-

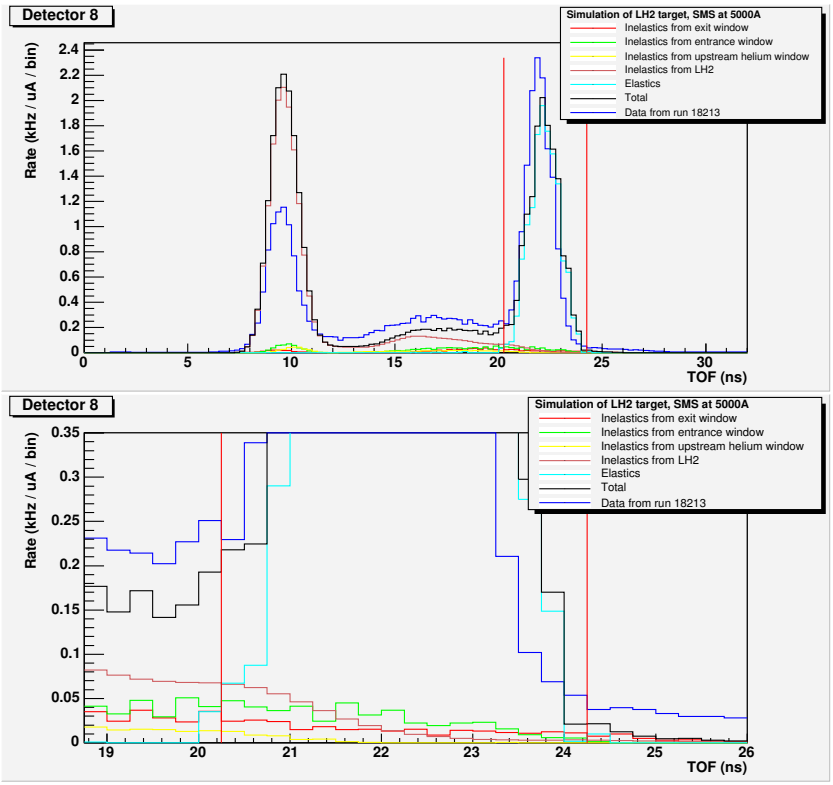

Figure 8: *Comparison of Monte Carlo and data for Octant 8, Detector 8 over whole TOF range (upper plot) and zoomed in on region beneath elastic peak (lower plot). Data appear in dark blue, total Monte Carlo appears in black, with the breakdown of contributions to the Monte Carlo displayed by the other colors. The windows contributions account for half of the background underneath the elastic peak, the other half arises from inelastic protons produced in the LH2. This last contribution is well measured in the normal LH2 run. Note that the size of the pion peak (left side) is set by the discriminator threshold (not tuned in the Monte Carlo) and that the pion data are not part of the proton analysis.*

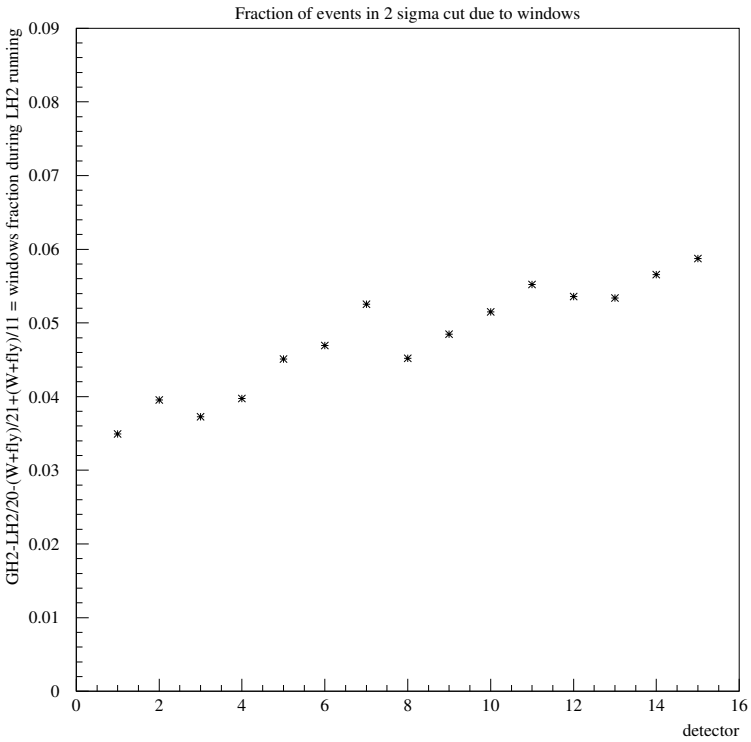

Figure 9: *Contribution of target windows to the rate within* $\pm 2\sigma$ *of the elastic proton peak for* LH_2*. The analysis was based entirely on the rescaling of empty target* (GH_2) *and flyswatter with radiator data (no simulation).*

tries in comparable regions of TOF with the LH_2 data will give us confidence in the systematic uncertainties in our subtraction scheme.

For further verification of this background subtraction scheme, we expect to rely on methods which proved successful for the January 2003 data: interpolation of the asymmetry in TOF, and running with the G^0 spectrometer magnet at lower field. The high statistical precision we will ultimately achieve in LH_2 will allow us to bin the asymmetry in TOF on either side of the elastic peak, and attempt to make interpolations beneath the peak. Additionally, running the spectrometer magnet at lower fields (4500 A current, as opposed to the standard 5000 A current) tends to shift elastic proton peak to higher TOF. This allows us to extract proton asymmetries in other regions of phase space neighboring the elastics. For the January 2003 data, it was found that the 4500 A asymmetry for TOF's populated by the elastic peak at 5000 A agreed with the interpolated asymmetry from 5000 A data alone. Supplementing the running on LH_2 with reasonable amounts of running on GH_2 and Al frame targets, and on the LH_2 target at reduced spectrometer field, will give us confidence in the systematic uncertainty due to background subtraction.

In Table 6, we present estimated overall uncertainties in the asymmetries from statistics and corrections due to background. They represent a snapshot of what we know in this early period of the actual data-taking. The background corrections are based on relatively simple interpolation schemes at this stage of the analysis. In all cases the central values of, e.g. background asymmetries, *are those taken from the present data*; the statistical uncertainties in all quantities are projected for the full run. The main difference between the present statistical precision and that in the G0 Technical Design Report (TDR 1993) is the effect of the increased beam polarization (49% assumed in the TDR, ~75% achieved). This is partly offset by a smaller azimuthal acceptance.

A simplified example of the analysis illustrates other important points. The measured asymmetry may be written as a sum of the elastic and background asymmetries, appropriately weighted

$$A_{meas} = \frac{A_{el} + f_{back} A_{back}}{1 + f_{back}}, \tag{4}$$

where f_{back} is the fraction of background events; solving for A_{el} gives

$$A_{el} = A_{meas}(1 + f_{back}) - f_{back} A_{back}. \tag{5}$$

The uncertainty in A_{el} is then

$$\Delta^2 A_{el} = (1 + f_{back})^2 \Delta^2 A_{meas} + (A_{meas} - A_{back})^2 \Delta^2 f_{back}^2 + f_{back}^2 \Delta^2 A_{back}. \quad (6)$$

The middle term is noteworthy. We observe large *positive* values, $A_{back} = \mathcal{O}(30 \text{ ppm})$, for the asymmetry of the background in the higher Q^2 detectors, increasing the value of the middle term. This is the main contribution to the larger uncertainties (relative to the proposal) in the table. The fluctuation of the values, e.g. in the right-hand column results from the use of the presently measured background asymmetries – we expect these values to have a smoother variation in the final analysis. We also note that the simplest interpolations for detector 15 (on which these estimates are based) are significantly more difficult because, unlike all the other detectors, the elastic events are essentially adjacent to the pion peak as shown in Figure 10.

Table 6: *Preliminary estimated uncertainties due to statistics and background corrections as a function of Q^2. The total uncertainty is the sum of the statistical and 'background' uncertainties added in quadrature. The 'TDR' (1993) uncertainties are adjusted for somewhat different Q^2 binning above $Q^2 = 0.5$ GeV^2. The irregular list of increases in the right-hand column is due mostly to the present statistical precision of the background asymmetries.*

Q^2 (GeV^2)	$A_{el,th'y}$ (ppm)	ΔA_{meas} (%)	ΔA_{back} (%)	ΔA_{el} (%)	$\Delta A_{el,TDR}$ (%)	Increase (%)
0.15	-3.3	4.4	3.6	5.6	4.6	22
0.22	-5.7	3.9	4.6	6.1	4.7	29
0.29	-8.5	3.9	6.5	7.6	4.3	76
0.35	-11	4.6	8.4	9.6	4.2	129
0.41	-14	3.7	3.9	5.3	4.3	24
0.54	-21	4.3	7.8	8.7	8.3	5
0.67	-28	3.8	7.8	8.7	6.2	40
0.84	-38	4.0	13.2	13.8	7.4	86

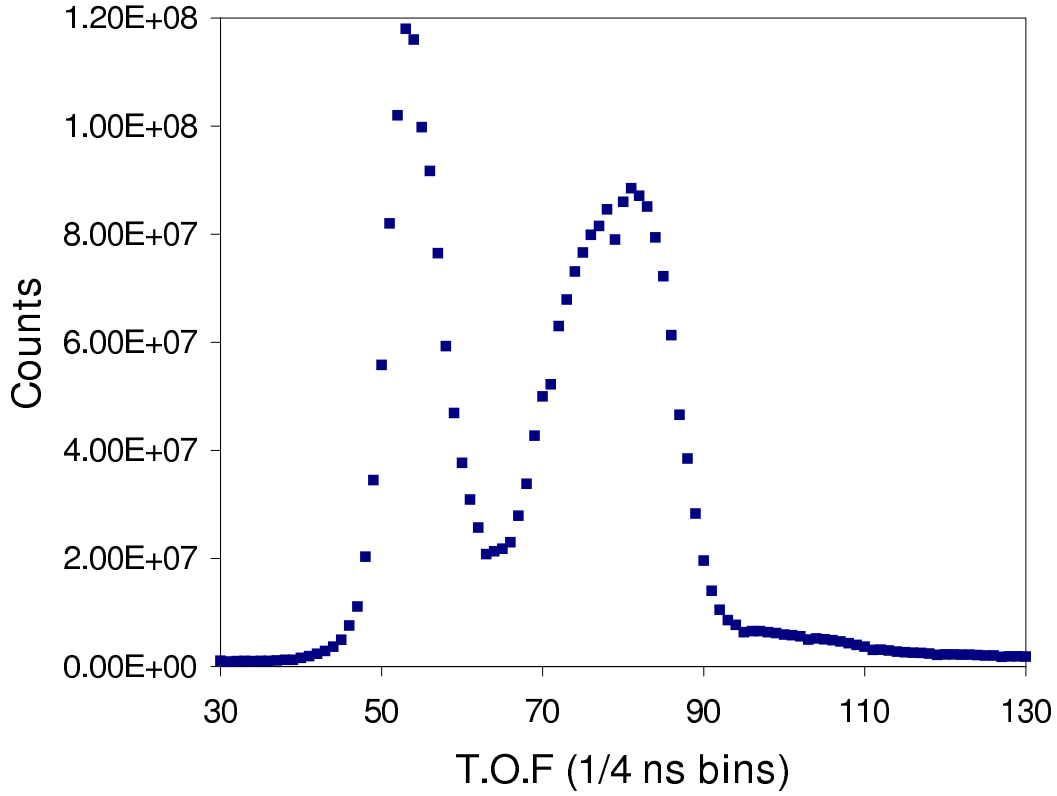

Figure 10: *Time-of-flight spectrum for detector 15. The peak on the left is the pion peak; the elastic 'bump' comprises protons corresponding to* Q^2 *from about 0.95 (left) to 0.45 (right)* GeV^2.

We expect some reduction in the background uncertainties as the result of more careful analysis and more accurate input (certainly in the asymmetry values, possibly from tuning the simulation to better match the observations). Finally we note that the TDR uncertainties in the forward asymmetry measurement constitute roughly 1/3 of the (squared) total uncertainty in G_E^s.

6 Status of the electronics, dead-time, noise to counting statistic.

Question 8 : What is the status of the custom detector electronics, both the North American and the French? Can helicity correlated dead time seen by the French electronics be reconciled with dead time observed in the North American electronics. What is the noise to counting statistics ratio of these systems?

1. Electronics performance:
   The performance of the Time Encoding (TE) electronics during the second engineering run is satisfactory. In the following two metrics of their performances are described.

   At each reading of the TE electronics, the modules themselves produce a bit signaling their performances during the last integration period. The malfunctions signaled by those bits are : unusable clock train due to bad external timing signal or marginal pulse structure for the North American case, and unacceptably high instantaneous high rates for the French case. The metric used on a regular basis to assess the performance of the electronics is the ratio of the number of readings without error bits over the total number of readings, defined as the efficiency. Figure 11 shows the efficiency of the French and North American modules during the data taking of January 04. The efficiency is overall 100% and a sign of the good performance of the electronics. The use of a more stable Y_0 and clock (beam synched timing signals) and improved level translators has significantly improved this situation since the first engineering run during which the North American efficency was of the order of 75 %.

   During the first engineering run, the differential non-linearity (DNL) of the North American time encoding was measured to be significantly larger than measured on the bench. Moreover, the differential non linearity was varying with time (fluctuating at the level of 10%). The impact of this effect was twofold. On one hand, the PID cuts as well as the dilution of the asymmetry by the background contribution were time dependent and would have required repetitive calibrations. In

addition, the precision of the binning in Q^2 of the data of detectors 15 (made through cuts in the time of flight (ToF) distribution) would have been significantly reduced. Once again, the use of better shaped Y_0 (start signal for the TE electronics) has significantly reduced this problem. Figure 12 shows reduction of the DNL between the first and second engineering runs. Finally, in order to insure the best resolution possible for the Q^2 binning of the data of detector 15, the signals off the North American detectors 14 and 15 are now read by both North American (ToF resolution 1ns) and French (ToF resolution 0.25 ns) modules. The commissioning of the new French modules is underway.

2. Dead-time
   The G^0 custom electronics have been designed to be able to measure high rates ($\sim$ 1 MHz of triggers) with a controlled dead-time. If an event produced by the beam burst (n), triggers[1] the electronics, any data produced by the next beam pulse (n+1) for the same channel, are not recorded, this system is called Next-Pulse-Neutralization (NPN). Both North American and French electronics feature the NPN system. In the following the probability of being dead is called f, it is proportional to the rates of events triggering the electronics and will cause the measured yield Y_M to differ from the true yield Y_T as :

$$Y_M = (1 - f)Y_T \tag{7}$$

   The overall deadtimes are about 10% for the North American and 15% for the French electronics (see Figures 13 and 14). Control of the dead-time is necessary for the success of the experiment because the number of events is expected to vary in a helicity correlated way arising from the charge asymmetry (A_Q). As a result of the dead-time effect, the resulting false asymmetry is :

$$A_{false} = -f \times A_Q \tag{8}$$

   In order to test our ability to correct for the dead-time effect, we have conducted two types of measurements with the full liquid hydrogen target.

[1] An event triggers the electronics if the four PMTs attached to one particular scintillators pair produces a signal in coincidence.

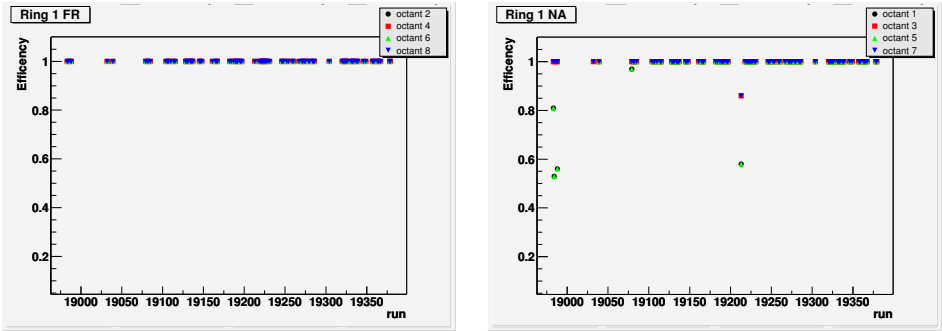

Figure 11: *Efficiency of detector 1 for the French and North American TE electronics during January 2004. At each reading, the electronic modules assess their own performance (see text) under the form of an error bit. The efficiency is ratio of reading without errors over the total number of reading.*

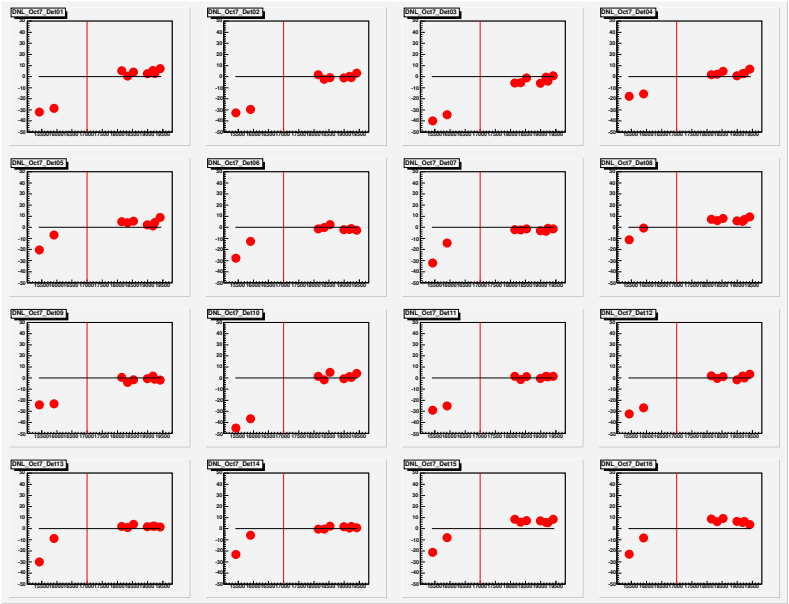

Figure 12: *Differential non linearity metric for North American modules versus run number for the sixteen FPD of Octant 7. This quantity represent the relative asymmetry of the even to odd bin withs of one ToF distribution. Runs from the first engineering runs are on the left side of the red line. Since the first engineering run, the DNL has been reduced in absolute and relative (run to run) amplitude.*

- Non Helicity correlated test :
  For this test the beam intensity is varied from 5 to 40 μA. The variation of the measured yield in each detector is evaluated under different type of corrections. In both the North American and the French cases, the dead-time corrections are twofold. In a first step the number of four fold coincidence is evaluated and corrected based on the NPN system. In a second step the number of "singles" where 1,2 or 3 PMTs are hit, is evaluated and the associated dead-time is corrected. For the North American case, the number of singles is evaluated from the Fastbus data stream, while in the French case the dead-time due to singles rates is evaluated from the Time Encoding electronics outputs and the Fastbus data stream. The two corrections are nevertheless equivalent and give similar results as shown in figure 13 for North American electronics and figure 14 for French electronics. Those figures show that the dead-time correction is understood at the same level of accuracy for the two sets of electronics. The higher sensitivity to the beam charge observed on the French electronics could be partly due to lower effective threshold which will be adjusted for the production runs. The best dead-time corrections to date under-correct[2] the dead-time effect by 1% at 40 μA. As a result, the false asymmetry rising from the dead-time effect after correction in the case of an accumulated charge asymmetry of the order of 1ppm, would be only 0.01 ppm even if no further corrections were applied. One should nevertheless note that the residual dead-time effect is further corrected by the linear regression procedure. This procedure is used to cancel the yield sensitivities to the position, angle and charge beam properties.
  The status of the dead-time corrections that has been described in the preceding section, is relevant for the setup of the NA electronics during this current engineering run. During the first engineering run (Nov 02 - Jan 03), an anomaly in the CFD's dominated over the expected dead-time losses. That anomalous behavior, which could be parametrized as a 70 ns effective dead-time (see figure 13) was corrected by changing the CFD's parameters. Fig-

[2]It was checked that the remaining dead-time cannot be attributed to a global reduction of the target density using the luminosity detectors located downstream of the target.

ure 13 shows that this effective dead-time corrections is now inappropriate.

- Helicity correlated test :
  The ultimate check of the validity of the dead-time correction is to measure directly the correlation between the measured asymmetry and the charge asymmetry, see equation 8. For this measurement, the charge asymmetry is driven to a large value using the IA cell. Figure 15 shows the linear dependence of the yield asymmetry as a function of the charge asymmetry without (black triangle) and with (red square) applying the dead-time correction. The results shown on figure 8 show that the dead-time correction reduces the factor f (see equation 8) from 10% to 1%. The correlation between the charge asymmetry and the measured asymmetry will be further reduced by the linear regression procedure.

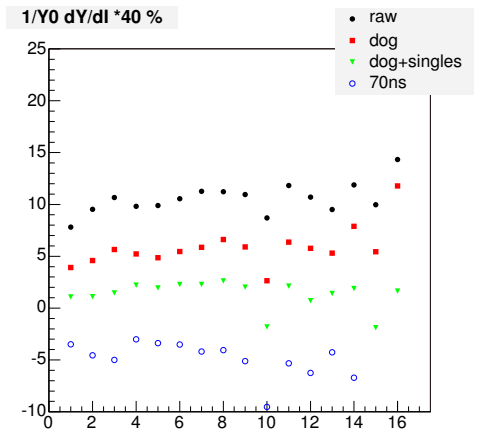

Figure 13: *North American yield variation with beam intensity under different dead-time corrections for the 16 detectors. The plotted quantity is the decrease of the yield per μA at 40 μA. The black dots are for data without any dead-time correction, the red square are for the data corrected from the four fold coincidence only, the green triangles are for the single and four fold coincidences correction. The blue open circles are for the old (out of date) effective dead-time corrections.*

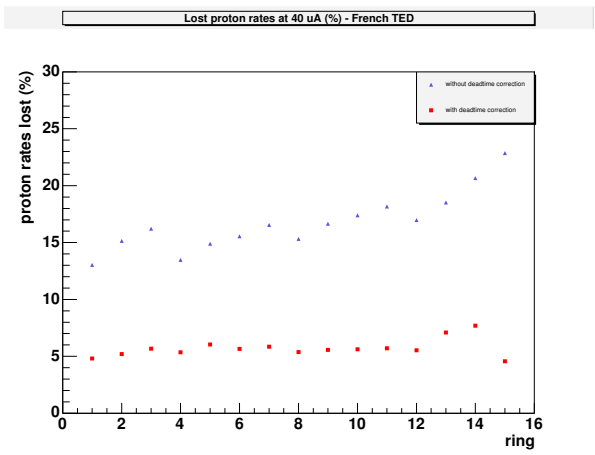

Figure 14: *French yield variation with beam intensity with (square) and without (triangle) dead-time corrections for the 16 detectors. The plotted quantity is the decrease of the yield per μA at 40 μA.*

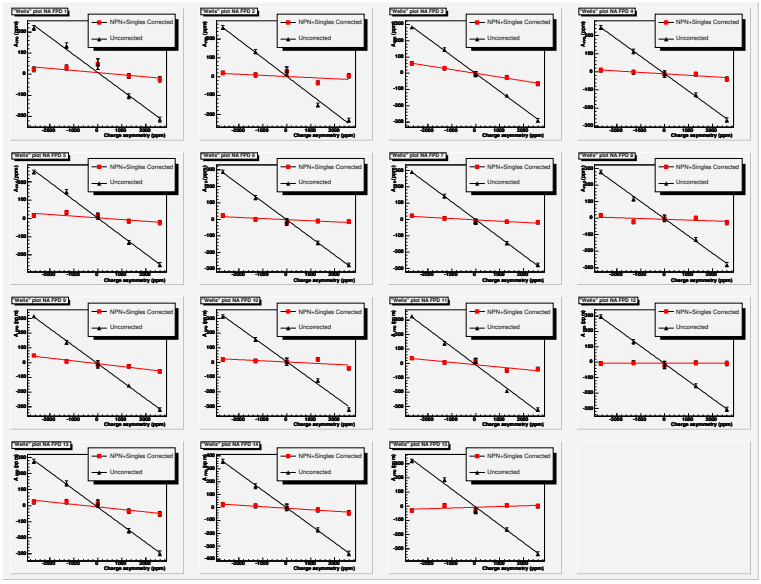

Figure 15: *Correlation between the measured asymmetry and the charge asymmetry as measured by the NA electronics. The charge asymmetry is driven to a large value using the IA cell. The black triangle show the uncorrected physics asymmetry and the red square show the dead-time corrected physics asymmetry. The linear regression will further reduce the dependency of the physics asymmetry with the charge asymmetry.*

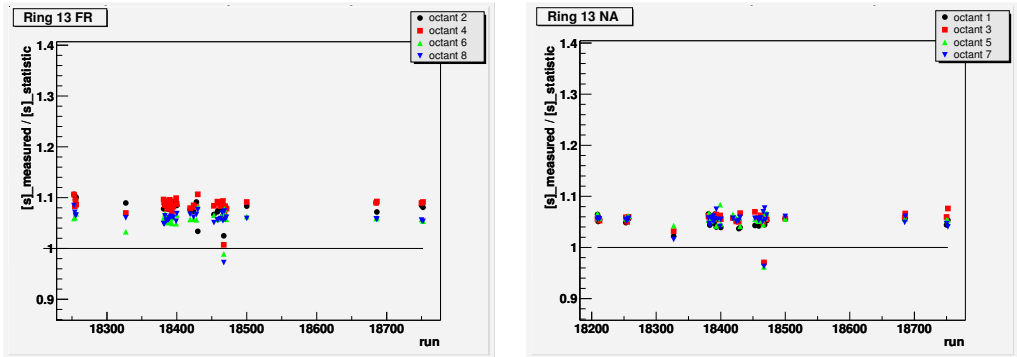

Figure 16: *Noise to statistical fluctuation for the North American and French detectors of ring 13 during the data taking on liquid hydrogen target in December 03.*

3. Noise to statistical fluctuation.
   In the case of a purely statistical measurement, the width of the distribution of measured asymmetry ($\sigma_{measured}$) is related to the number of events (N) recorded during each helicity period by :

$$\sigma_{measured} = \frac{1}{\sqrt{N_- + N_+}} \tag{9}$$

   Any additional noise other than statistical increases the width of the measured asymmetry. The figure 16 a show the noise to counting statistic ratio for the French and NA electronics respectively for ring 13 for the data taken on liquid hydrogen target in December 03. For this calculation, the number of count (N) is corrected for dead-time. This ratio is of the order of 1.1 for all detectors. The noise due to the number of counts for each detector is on the order of 1500 ppm. It has been shown that the noise produced by the target density fluctuation is 300 ppm and that the Beam Current Monitors used for this analysis have a noise of 300 ppm. Those two contributions account for 4% of the 10% noise above counting statistic, 6% remaining yet un-explained. In any case, the level of noise to expected statistical fluctuation, will ultimatly decrease the statistical precision of the G^0 measurement by 10% compared to the proposal which is negligable.

7 Status of Y_0 timing.

Question 9 : What is the status of the "YO" timing? Is it clear that using this as a common stop to the TDC's benefits the experiment?

We now have operational experience with the Y_0 and CLK signals from the "Musson box". Parameters have been tuned so the behavior is now flawless. Acceptable clock trains arrive at the time-encoding electronics without a single exception through days of running under a wide variety of beam conditions.

The Musson Box produces two beam-synched signals (CLK and Y_0) which are synchronized to the arrival of the beam in Hall C rather than to the laser-pulse time at the source. This is intended to eliminate possible small helicity-correlated offsets in the start-time used to calculate the time-of-flight of particles from the target to focal plane detectors. If not corrected or eliminated, helicity-correlated time offsets of several femto-seconds (averaged over the entire run) could introduce false asymmetries of order of parts per million into the count of events within time-of-flight cuts. A concern which must be addressed is whether the Musson Box system (and associated beam pick-offs) might introduce an unacceptable helicity-correlated time offset due to sensitivity to another helicity-correlated beam property such as intensity or beam position. The Musson Box derives the timing for the 31.1875 MHz Y_0 signal (and the 499 MHz CLK signal) from a 1497 MHz RF cavity signal. A 31.1875 MHz stripline BPM is used only to resolve the 48-fold ambiguity of mapping the 1497 MHz signal to the 31.1875 MHz beam-arrival. Helicity-correlated time offsets could in principle be introduced by dependence of the cavity signal on the beam properties.

Sensitivity to beam parameters was measured by using a TDC to compare the Y_0 time with the time of a 31.1875 MHz signal produced from the master oscillator. The bin width of the TDC is approx. 35 ps and 31 measurements are made and averaged together for each macro-pulse (every 1/30 seconds). The intrinsic resolution of each measurement then is about 2 ps.

The plot 17 shows this Y_0 TDC time as a function of beam position X and Y. No dependence is seen and an upper limit can be set in each case. Very conservatively the limit on position dependence can be said to be less than 10 ps over a range of 0.5 mm or less than 20 ps/mm in each case. If we then assume the maximum acceptable helicity-correlated beam position shift of 20 nm, we see that any position-dependence of the cavity signal will

introduce a time shift of not more than 20 nm * 20 ps/mm = 0.40 fs, which is small enough to be acceptable.

Figure 18 show attempts to measure dependence of Y_0 time on beam current. Again no dependence on beam current is visible. The jump at 5 μA is due to a feature of the box which causes it to switch to an alternate time reference if beam signals are too weak. The threshold for this transition is set at 5 μA. A very conservative upper limit on beam-current dependence can be set at 35 ps time shift across the 30 μA range covered. The maximum acceptable helicity-correlated beam current dependence is 1 ppm at 40 μA (40 pico amp shifts). This gives an upper limit on the time shift of (35 ps/ 30 μA)*40 pA or less than 0.050 fs, which is again much smaller than what we are concerned with.

An additional test has been performed in which the electron orbit is changed (using a dogleg) to demonstrate that the resulting change in arrival time of the electrons in the hall (approx. 5 ps) is reflected by a change in time of the Y_0 and CLK signals. The test demonstrates that the Musson box responds as expected and with approximately the correct magntitude. Analysis is continuing in the Accelerator Division (Musson and Freyberger); the accuracy limitation may be knowledge of the size of the orbit change. It should be noted that more demanding and quantitative tests have been successfully carried out on the bench. Static tests with a vector voltmeter have demonstrated that the Y_0 time tracks the time of the 1497 MHz input signal, as designed. Transient tests using a Dynamic Signal Analyzer to apply 30 Hz square-wave offsets of 23 ps showed the Y_0 tracked the changes with an 80 μs response time. In a dynamic test, a 30Hz modulation was applied to a phase shifter on the 1497 MHz input signal to impose a 1 ps shift with a 30 Hz frequency. The 30 Hz signal was then detected in the internal control voltage (V_{31}^{ctrl}) demonstrating that the box was responding to the delay as expected.

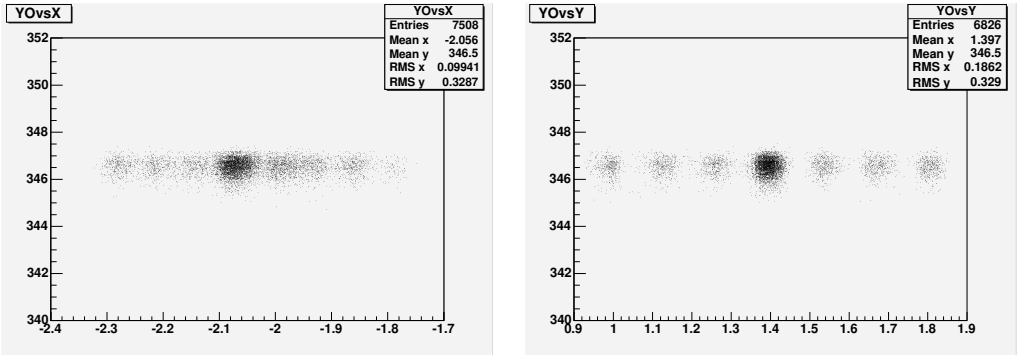

Figure 17: *Y_0 TDC time as a function of beam position X and Y respectively. The vertical axis in each plot is in TDC bins (35 ps) and the horizontal is in mm. No dependence is seen and an upper limit can be set in each case.*

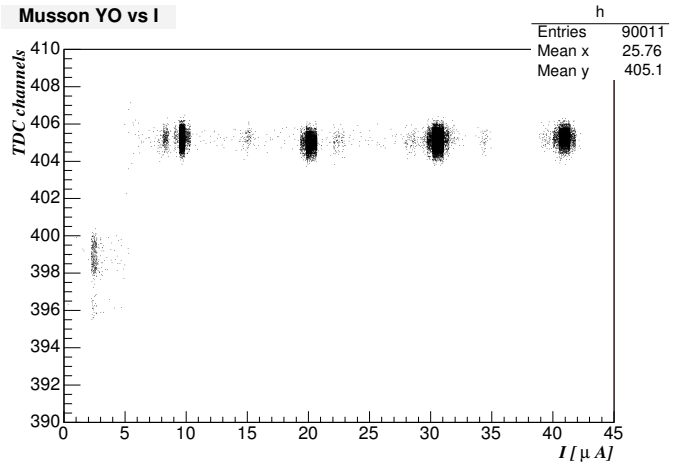

Figure 18: *Attempts to measure dependence of Y_0 time on beam current. TDC channel (35 ps/channel) as a function of average beam current (averaged over a 1/30 s macropulse). No dependence on beam current is visible. The jump at 5 μA is due to a feature of the box which causes it to switch to an alternate time reference if beam signals are too weak. The threshold for this transition is set at 5 μA.*

8 Current Dependence of Beam Polarization.

Question 10 : During the second engineering run a test is planned to measure the beam polarization ranging from low current measurements to high current production runs. If this test was successful, is there any quantitative change to the beam polarization at high current, and if so, will it affect the G0 data quality?

The Hall C/Basel Møller Polarimeter is capable of measurements of the beam polarization with systematic uncertainties of better than 1% [1]. A series of studies carried out during the first G0 engineering run which tested the effects of beam mis–steering, laser phase, potential target "wrinkling" effects, etc. gave results consistent with this expectation. The results from the Møller tests during this run were remarkably stable and the whole body of data was statistically consistent.

The last remaining significant question regarding polarimetry for G0 pertains to current dependence. G0 will typically run at 40 μA while the Møller polarimeter usually operates at 1–2 μA. While there is no reason to expect that the beam polarization should vary with beam current, Møller measurements at currents on the order of 10 μA would give one more confidence that there are no current dependent effects.

This fall, we carried out two tests aimed at examining the beam polarization at higher currents. The first entailed the use of a thinner Møller target in combination with the Møller beam rastering system to measure the polarization up to $\approx$ 10 μA. Results of this test are shown in Fig. 19. We first tested that the new 1 μm foil yielded results consistent with the previously used 4 μm foil. We then took a series of measurements, varying the beam current from 2 to 10 μA. The Møller raster was used to ensure that depolarization of the target foil due to beam heating would remain significantly less than 1%. As seen in Fig. 19, the beam polarization shows no discernible current dependence.

The second test performed during this engineering run was actually the commissioning of a new beam kicker and iron wire target system. While we were not counting on the results of this test to demonstrate the current–independence of the beam polarization, they end up giving some nice supporting evidence that this is indeed the case.

The kicker is a magnet placed about 45 m upstream of the Møller target

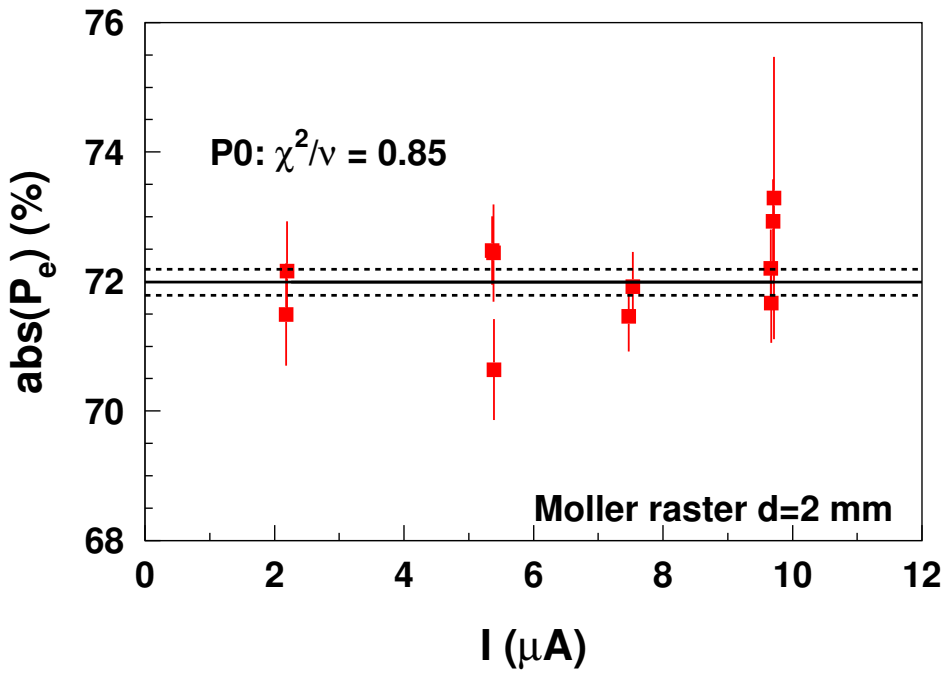

Figure 19: *Beam polarization as measured with the Hall C Møller polarimeter as a function of beam current. For these measurements, a 1 μm iron foil target was used in combination with the Møller raster system. The Møller raster diameter was ≈2 mm. The solid line denotes a fit to a constant with* $\chi^2/\nu = 0.85$.

that provides a ≈1–2 mm vertical kick to the electron beam. The total time for the kick is 20 μs and the frequency can be varied from 100 Hz to 10,000 Hz. In combination with the 25 μm diameter iron wire target, the low duty factor of the kicker magnet allows us to avoid undue heating of the target and thus take Møller measurements at even higher currents. Results from the first commissioning run of this device are shown in Fig. 20. While the results from the kicker running are not of the statistical precision normally achieved in Møller runs (this was due to the required low duty factor necessary to keep the wires from getting too hot combined with a

somewhat larger than expected random coincidence background) one can see that these results indicate no apparent current dependence of the beam polarization up to 20 μA. The two highest current runs, with a combined statistical uncertainty of 2.7%, are totally consistent with the data taken at $\approx 2\mu$A.

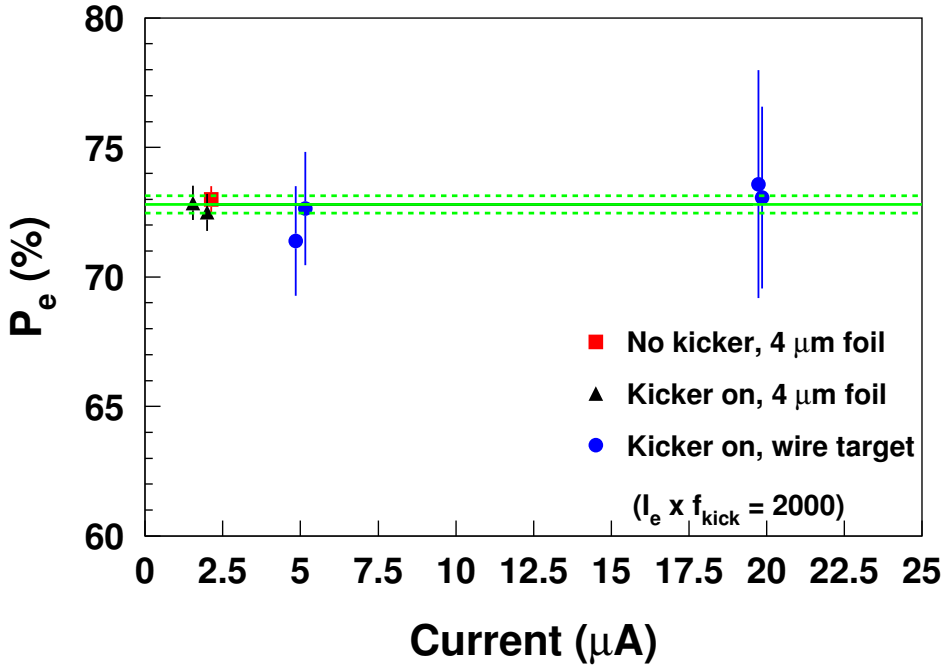

Figure 20: *Preliminary results from the first commissioning run of the Møller kicker and iron wire target system. The solid blue circles denote runs taken with the kicker magnet and iron wire target, while the black triangles are runs taken with the kicker on, but using an iron foil target. The red square is a run with no kicker on a standard foil target. All results have been corrected for Hall A bleed-through. Note that the average polarization is a bit larger than in Fig. 19 - this is likely due to a spot–move that occurred between the two measurements.*

In summary, the results from our high current Møller measurements us-

ing the new thin 1 μA target and Møller raster indicate no dependence of the beam polarization on current up to 10 μA. The new kicker and iron wire target system also sees no current dependence up to $\approx 20\mu$A, although with larger statistical uncertainties. The combination of these two results gives us confidence that our polarization measurements typically taken at ≈ 2 μA will accurately characterize the beam polarization at higher currents. G0 will not need to assign any extra systematic uncertainty on the beam polarization stemming from concerns about differences in beam currents used for production running and polarization measurements.

9 Experience reliability.

Question 11 : Has the G0 equipment performed sufficiently reliable for a full production run to take place?

Yes, in December 03 and January 04 there were no major cause of down-time related to the G^0 equipment. As any other running experiment, we undergo a couple hours or so of DAQ related issues a week, which to date constitute our most frequent downtime. We have experienced five or so SMS magnet events since December : three were caused by irregularities in the Helium supply and two by the PLC locking up. We have no significant down time created by the target, the electronics or the detectors.

10 Conclusion.

Based on the responses above, as well as our own studies, we conclude that the G0 experiment is ready to take its production data. The experimental apparatus now works very reliably, with only small amounts of down-time due to largely to magnet and DAQ problems (few hours/week). The helicity-correlated beam properties are now within the specification with the feedback operational, and will make a small contribution to the overall uncertainty. The background yields and asymmetries are being determined with a combination of LH2, GH2 and Al target measurements, allowing us to work around the loss of the flyswatter target and will increase the statistical uncertainty in the asymmetry by 50% at most; thereby increasing the overall uncertainty in G_E^s by of order 15% or less and having a much smaller impact on G_M^s.

References

[1] M. Hauger *et al.*, Nucl. Instrum. Meth. A **462**, 382 (2001).